



UNIVERSITY OF LEEDS

This is a repository copy of *Steam generation in a nanoparticle-based solar receiver*.

White Rose Research Online URL for this paper:

<http://eprints.whiterose.ac.uk/104305/>

Version: Accepted Version

Article:

Jin, H, Lin, G, Bai, L orcid.org/0000-0001-9016-1569 et al. (2 more authors) (2016) Steam generation in a nanoparticle-based solar receiver. *Nano Energy*, 28. pp. 397-406. ISSN 2211-2855

<https://doi.org/10.1016/j.nanoen.2016.08.011>

© 2016 Elsevier Ltd. Licensed under the Creative Commons

Attribution-NonCommercial-NoDerivatives 4.0 International

<http://creativecommons.org/licenses/by-nc-nd/4.0/>

Reuse

Unless indicated otherwise, fulltext items are protected by copyright with all rights reserved. The copyright exception in section 29 of the Copyright, Designs and Patents Act 1988 allows the making of a single copy solely for the purpose of non-commercial research or private study within the limits of fair dealing. The publisher or other rights-holder may allow further reproduction and re-use of this version - refer to the White Rose Research Online record for this item. Where records identify the publisher as the copyright holder, users can verify any specific terms of use on the publisher's website.

Takedown

If you consider content in White Rose Research Online to be in breach of UK law, please notify us by emailing eprints@whiterose.ac.uk including the URL of the record and the reason for the withdrawal request.

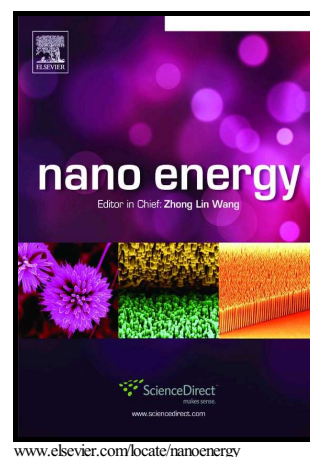


eprints@whiterose.ac.uk
<https://eprints.whiterose.ac.uk/>

Author's Accepted Manuscript

Steam generation in a nanoparticle-based solar receiver

Haichuan Jin, Guiping Lin, Lizhan Bai, Aimen Zeiny, Dongsheng Wen



PII: S2211-2855(16)30294-4
DOI: <http://dx.doi.org/10.1016/j.nanoen.2016.08.011>
Reference: NANOEN1424

To appear in: *Nano Energy*

Received date: 12 April 2016
Revised date: 15 July 2016
Accepted date: 3 August 2016

Cite this article as: Haichuan Jin, Guiping Lin, Lizhan Bai, Aimen Zeiny and Dongsheng Wen, Steam generation in a nanoparticle-based solar receiver, *Nano Energy*, <http://dx.doi.org/10.1016/j.nanoen.2016.08.011>

This is a PDF file of an unedited manuscript that has been accepted for publication. As a service to our customers we are providing this early version of the manuscript. The manuscript will undergo copyediting, typesetting, and review of the resulting galley proof before it is published in its final citable form. Please note that during the production process errors may be discovered which could affect the content, and all legal disclaimers that apply to the journal pertain.

Steam generation in a nanoparticle-based solar receiver

Haichuan Jin^{a,b}, Guiping Lin^a, Lizhan Bai^{a,b}, Aimen Zeiny^b, Dongsheng Wen^{a,b,*}

^aLaboratory of Fundamental Science on Ergonomics and Environmental Control, School of Aeronautic Science and Engineering, Beihang University, Beijing 100191, PR China

^bSchool of Chemical and Process Engineering, University of Leeds, Leeds, LS2 9JT UK

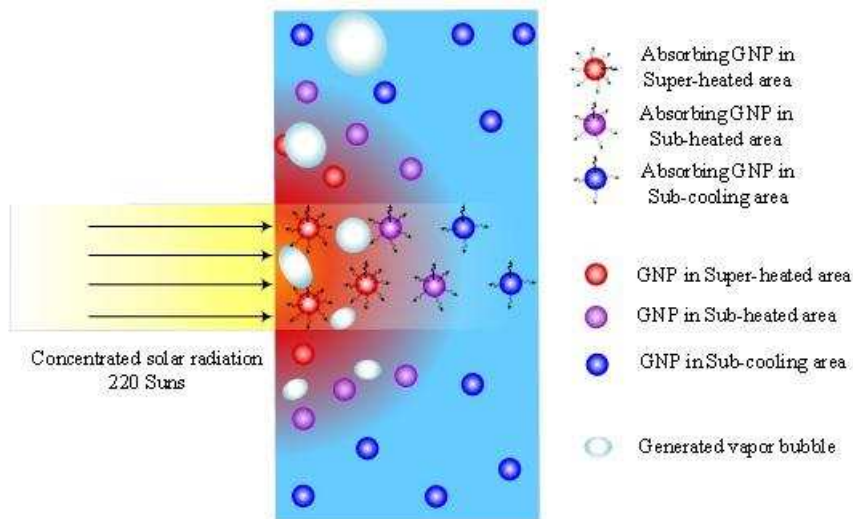
*Corresponding authors. Dongsheng Wen, Tel.: +0044 113 3432678; fax: +0044 20 78825003.

E-mail: d.wen@leeds.ac.uk

Abstract

Steam production is essential for a wide range of applications, and currently there is still strong debate if steam could be generated on top of heated nanoparticles in a solar receiver. We performed steam generation experiments for different concentrations of gold nanoparticles dispersions in a cylindrical receiver under focused natural sunlight of 220 Suns. Combined with mathematical modelling, it is found that steam generation is mainly caused by localized boiling and vaporization in the superheated region due to highly non-uniform temperature and radiation energy distribution, albeit the bulk fluid is still subcooled. Such a phenomenon can be well explained by the classical heat transfer theory, and the hypothesized ‘nanobubble’, i.e., steam produced around the heated nanoparticles, is unlikely to occur under normal solar concentrations. In the future solar receiver design, more solar energy should be focused and trapped at the superheated region while minimizing the temperature rise of the bulk fluid.

Graphical abstract



Keywords: nanoparticle, steam generation, nanobubble, solar energy, volumetric receiver

1. Introduction

Steam production is essential for a wide range of applications from large scale electricity generation, energy storage, desalination systems and refrigeration units to compact small scale systems such as sterilization and cleaning [1–4]. Conventionally steam is produced by the combustion of fossil fuels or direct heating from electricity, which is environmentally unfriendly. Employing solar energy, an abundant, clean and renewable energy source, for steam production is a rapidly developing area [5–8]. Currently solar-based steam production (i.e., either solar trough or solar tower systems) is based on heating a bulk fluid to its boiling temperature under high optical concentrations. The steam generation efficiency heavily relies on the surface temperature and radiation properties of the absorber, whose high temperature needed for bulk steam production leads to large heat loss to the ambient and low energy efficiency.

It has been reported recently that certain nanoparticles, especially those with Localized Surface Plasmon Resonance (LSPR) properties [9,10], can absorb solar energy efficiently in a liquid medium [11–14]. For an aqueous nanoparticle dispersion [15], it would lead to a rapid increase of the particle temperature and steam production, albeit the bulk fluid was still in the subcooled state [16,17]. For example, the research team from Rice University showed that by using a very dilute gold nanoparticles dispersion, i.e., 16.7 ppm, under focused sunlight via a Fresnel Lens, rapid steam production was realized while the bulk fluid temperature was still at ~ 6 °C [11]. The calculation showed that the steam generation efficiency was reached up to 80%, and only a small portion of the solar radiation was used to increase the bulk fluid temperature. Similar to the concept of energy localization on the surface [18], it appears that solar energy was localized by the nanoparticles. It was further hypothesized that rapid heating of nanoparticles produced nanobubbles immediately around the nanoparticles, and the rise of nanobubbles to the top surface of the liquid realized the release of the vapor produced [19–21]. Subsequent simulation work [11,16,17,22] showed the possibility of nanobubble formation based on a non-equilibrium phase change assumption.

The heating of nanoparticles and formation of nanobubbles have become an intensive research topic in the medical area. It has been confirmed both experimentally and theoretically [13,14,16,23–25] that under an intensive laser heating (i.e. > 1000 MW/m²), bubbles can be generated around the heated nanoparticles [26,27]. By controlling the laser power and pulse appropriately, the growth and contraction of bubbles can be very fast, which is associated with the propagation of pressure waves that could bring thermal-mechanical damage to surrounding cells at a dimension much larger than that of a single nanoparticle [28]. However, it is still unclear if bubbles can be formed under a relatively low heat flux provided by concentrated

sunlight (i.e., typically $<1 \text{ MW/m}^2$), and a few concerns have been raised recently. For instance, Ni et al. [29] showed that there were no nanobubbles produced under a solar concentration of 10 Suns, and suggested that the classical global heating may be responsible for the steam generation. Through a molecular dynamics simulation study, Chen et al. [19] also showed that it was difficult to form nanobubbles under continuous heating conditions even under a high heating power.

It shall also be of note that most of the solar steam generation experiments employed only one point temperature measurement [11,29,30], without knowing the temperature distribution of the fluid, which may lead to misleading or unconvinced conclusions. Clearly there is still a critical lack of both strict experimental evidence and well-accepted mechanism analysis in the solar steam generation. Aiming to address these contradictions, steam generation using gold nanoparticle dispersions with different concentrations in a cylindrical tube under focused natural sunlight was investigated experimentally, and a 3-D mathematical model was also established to reveal the non-uniform temperature distribution inside the nanoparticle dispersions. We revealed that steam generation during the heating up stage was mainly caused by localized boiling and vaporization in superheated regimes due to a highly non-uniform temperature distribution, albeit the bulk fluid is still subcooled. Such a phenomenon can be explained by the classical heat transfer theory and the hypothesized nanobubble, i.e., steam produced around heated particles, was unlikely to occur under normal solar concentrations.

2. Experimental details

2.1. Nanoparticles fabrication and characterization

A one-step method [31] was employed to produce stable gold nanoparticles (GNPs) dispersions. First, 5×10^{-6} mol HAuCl_4 (Sigma-Aldrich) was dispersed into 190 ml DI water in a three-necked flask, then a magnetic blender with a heating source was used to stir the liquid until the occurrence of boiling. 10 mins later, 10 ml aqueous sodium citrate (Sigma-Aldrich) solution with a mass concentration of 0.5% was added into the prepared HAuCl_4 solution. The mixed solution turned dark blue within 30 s, and the final color became wine red after being heated for an additional 20 mins. The GNPs dispersions maintained good stability for over two months, and were used for the experiments without further purification and separation. Gold nanoparticles' size and shape were characterized (Fig. 1A and B) by the Transmission Electron Microscopy (TEM) (FEI Tecnai TF20: FEGTEM Field emission gun TEM/STEM fitted with HAADF detector, Oxford Instruments INCA 350 EDX system/80 mm X-Max SDD detector and Gatan Orius SC600A CCD camera). A dynamic light scattering (DLS) device (Malvern nanosizer) was employed to identify the particle size distribution, which is presented in the Supporting Information.

2.2. Experimental setup

The experiments were performed under focused natural sunlight (Fig. 1C and D). Diluted GNPs dispersions (with concentrations of 1.02 ppm, 5.1 ppm and 12.75 ppm) and DI water were placed into four cylindrical tubes (i.e., inner diameter of 25 mm and length of 300 mm), respectively. The tubes were custom-made from high temperature resistant quartz, and vacuum interlayers were employed to reduce the convection heat loss to the ambient as much as possible (Fig. 2). The outer tube with a diameter of 60 mm had two small-bore pipes, which were used to fix the thermocouples. Fresnel lenses (400 mm \times 400 mm) with a 620 mm focal distance were used to focus the natural sunlight. The smallest focused spot has a diameter of 30 mm, and the

focused solar intensity in the experiments was 220 Suns. A solar radiation intensity sensor (SPN1, Delta-T Devices) with a measurement uncertainty of 2% was employed to measure the solar intensity.

In order to investigate non-uniform temperature distribution within the fluid, three type T thermocouples (Omega TT-T-40-SLE) with precision of ± 0.5 °C were placed in the bottom, middle and top of the test sample fluids, respectively. Another two thermocouples were placed inside and outside the cylindrical tube to measure the steam and ambient temperatures, respectively (Fig. 2). A microbalance (OHAUS Adventurer) was employed to measure the mass change of fluid when illuminated, where a water cooling system was used to condense the generated steam (Fig. 1D). Before the experiments, all the four cylindrical tubes were cleaned carefully with pure water at ambient temperature. These tubes with test sample fluids were then heated simultaneously under the same solar conditions (220 Suns). Due to the movement of the Sun and the change of liquid position because of steam generation, the focus point was manually adjusted to keep it on the fluid.

3. Results and discussions

3.1. Temperature profile

Once the tube was illuminated under 220 Suns, fluid temperatures rose immediately (Fig. 3), and main observations can be summarized as follows:

- (1) It was difficult for DI water to reach boiling under such a solar intensity (i.e. 220 Suns).

For DI water (Fig. 3D), the highest temperature was increased to only 65 °C (TC3) after 5 minutes' illumination. One position reached 90 °C after 10 minutes' illumination, then it remained nearly constant, indicating the attainment of a steady state where the heat loss was equal to the absorbed solar radiation energy.

- (2) All GNPs dispersions reached the boiling temperature fast and then remained unchanged at that value. Increasing the volume concentration could reduce the time required to reach the boiling point. For 1.02 ppm GNPs dispersion (Fig. 3A), it took more than 3 min for all the three measured positions to reach the boiling point. While for higher concentrations such as 12.75 ppm (Fig. 3C), it was reduced to only 90 seconds.
- (3) Large temperature differences existed within the fluid before reaching the boiling point, and the temperatures at the measured positions was highly non-uniform for all the sample fluids. For instance, an impressive temperature difference was observed, i.e., 46.5 °C between TC1 and TC3, in less than 1 minute's illumination for 12.75 ppm GNPs dispersion. However, for all GNPs dispersions, the temperature non-uniformity became much smaller after reaching the boiling point.
- (4) Steam can be generated under subcooled conditions and was highly particle concentration dependent. For 1.02 ppm and 5.1 ppm GNPs dispersions, appreciable steam temperature increase was only detected when the bulk fluid temperature reached approximately the boiling point (as shown by arrows in Fig. 3). However, for 12.75 ppm GNPs dispersion, almost immediately air temperature rise inside the tube was observed, indicating that vapor was generated rapidly. At that time, all the three thermocouples indicated that the bulk fluid temperature was still very low and impossible for boiling to happen. This suggested that vapor was produced when the bulk fluid was in the subcooled state, similar to the results reported by the research group from Rice University [11].

3.2. Steam production characterization

During the experiments, it was observed that after a few minutes' illumination, most of the bubbles were originated around the top of the inner surface of the tube, or from the thermocouple

wires. The initial generation of bubbles was related to the presence of nucleation sites on these rough surfaces, which benefits the embryo bubble nucleation and growth without large superheat. Once the surrounding temperature reached the boiling point, a large amount of vapor bubbles were generated continuously from the thermocouple wires located just below the focused point, where solar radiative energy would be converted into thermal energy leading to a high energy localization, and superheat can be easily reached. An example of a bubbling process in a subcooled bulk fluid is shown in Fig. 4 (i.e., video in Supporting Information) where three stages can be identified: the bubble formation, growth and release. When bubbles passed the focused area, the growth rate was obviously accelerated. The generated vapor was condensed to liquid, and the remaining GNPs dispersions were also analyzed, which showed no evidence of any chemical modification.

The evaporated water mass loss in dimensionless form (i.e., evaporated water mass divided by the total sample fluid mass before the experiment) is shown in Fig. 5. Clearly GNP dispersions showed much larger mass loss. Similar to the temperature profile, the mass loss was also highly dependent on the nanoparticles concentration. For instance, only 10% reduction was observed for DI water after 30 minutes' radiation, while 9 times more water was evaporated for the 12.75 ppm GNP dispersion in 25 minutes. It should also be noted that for the first 5 minutes, the difference in the mass loss was small for all GNP dispersions with different concentrations, albeit all the thermocouples indicated the attainment of the boiling temperature. This shall be related to the re-condensation phenomena due to the initial cold conditions of the tube inner surface, where most of the vapor was likely to be re-condensed. Nearly constant vaporization rate was observed after the initial 5 min, which indicated the presence of saturated boiling in the tube.

We quantified the amount of solar energy consumption for heating the fluid (P_{heating1}) and producing steam (P_{steam1}) during the heating-up process (i.e., subcooled stage), and energy consumption for producing steam (P_{steam2}) during the saturation boiling stage (i.e., Fig. 5 gray area) by the equations below (where the uncertainty analysis is provided in Supporting Information):

$$P_{\text{heating1}} = \frac{(c_w m_w + c_n m_n) \Delta \bar{T}}{\Delta t} \approx \frac{c_w m_w \Delta \bar{T}}{\Delta t} \quad (1)$$

$$P_{\text{steam1}} = \frac{r_w \Delta m_{w1}}{\Delta t} \quad (2-a)$$

$$P_{\text{steam2}} = r_w \dot{m}_w \quad (2-b)$$

where c_w and c_n are the specific heat capacity of water and gold nanoparticle, respectively; m_w and m_n are the total mass of water and nanoparticle, respectively; $\Delta \bar{T}$ is the averaging temperature increase of the three thermocouples within the sample fluids, representing the increment of bulk temperature; Δt is defined as the time needed for the first thermocouple temperature to reach the boiling point (100 °C) from the beginning of the experiment; r_w is the evaporative latent heat of water, Δm_{w1} is the vaporized mass loss during period of Δt ; \dot{m}_w is the evaporated water mass loss rate due to vaporization during the saturated boiling stage, which is defined as $\dot{m}_w = \Delta m_{w2} / \Delta t_{15 \text{ min}}$ (where Δm_{w2} is the mass loss during 15 min), which remains at a relatively constant value during the period of 10 ~ 25 minutes for all sample fluids, as shown in the stable mass change zone in the gray area of Fig. 5);

The calculated results are shown in Fig. 6, which indicates that adding gold nanoparticles into water increased the power for both heating the fluid and steam generation dramatically. For example, for 12.75 ppm gold nanofluid, $P_{\text{heating1}} = 97.3 \text{ W}$, almost 7 times higher than that of water. The calculated energy consumption in Fig. 6 also exhibits that the converted solar energy is mainly consumed to heat up the bulk fluid in the heating-up stage. However, the consumed

power for steam production should be higher if heat leak and re-condensation are considered: i) heat leak in steam generation was much higher than that in a bulk heating due to higher temperature at the top surface; and ii) a certain amount of steam was re-condensed and stayed on the inner wall of the tube, which was not measured by the scale. It shall be noted that after the bulk fluid reached the boiling point, most of the solar energy would be used for steam production.

In a separated study, Neumann et.al [11] observed that 80% of the solar energy absorbed by the nanoparticles dispersions was used for steam generation, and only 20% was for sensible heating. However, it shall be cautious to interpret these data considering the extremely non-uniform temperature distribution within the fluids. In their work, the sensible heat contribution was calculated from one-point temperature measurement in a cold region, which may easily under-estimate the enthalpy increase of the bulk fluid. In this paper, the sensible heating contribution based on the average temperature and only one thermocouple were calculated (Table .1). Clearly it shows that the sensible heating contribution can be significantly underestimated if only one temperature measurement was used. For example, the sensible heating efficiency during the heating-up stage based on only TC1 is 11.7% for 1.02 ppm gold nanofluid, less than one third of that from the average temperature, which is 37.9%. The relative contribution between the sensible heating and vapor generation becomes 64:36 for TC1 only, and 85:15 for the averaged three temperature measurement. If a colder regime temperature was used, more sever underestimation of the sensible heating contribution would occur, leading to a large steam production efficiency, due to the large non-uniform temperature distribution

3.3. Photothermal Conversion Characteristics

Considering the energy balance, the solar energy utilization efficiency is expressed as the photothermal conversion efficiency (PTE) η for both GNP dispersions and DI water, which is calculated by dividing the absorbed solar energy over the total incident solar radiation:

$$\eta(t) = \frac{(c_w m_w + c_n m_n) \Delta \bar{T} + \int_0^t r_w \dot{m}_w(\tau) d\tau}{\eta_f \int_0^t I A d\tau} \approx \frac{c_w m_w \Delta \bar{T} + \int_0^t r_w \dot{m}_w(\tau) d\tau}{\eta_f \int_0^t I A d\tau} \quad (3)$$

where A is the area of Fresnel Lens, $\eta_f \approx 90\%$ is a modest optical efficiency for Fresnel Lens without optimization [32,33]. The efficiency was calculated based on the heating-up stage, including the contribution from both sensible heating and steam generation over the period between the beginning of the experiment and the point when the first thermocouple reached the boiling point for GNP dispersions. For DI water, the time interval for the calculation was determined as 8 minutes from the beginning of the experiment, because no thermocouple reached the boiling temperature. The photothermal conversion efficiency (Fig. 7) under 220 Suns illumination increased nonlinearly with the increase of the volume concentration of GNP dispersions, and a shift happened when the concentration reached a certain value. A maximum PTE of 80.3% is obtained for 12.75 ppm GNPs dispersion. To quantify the capability of gold nanoparticles in absorbing solar energy, the specific absorption rate (SAR) is calculated [34]:

$$\text{SAR} = \frac{(c_w m_w + c_n m_n) \Delta \bar{T}_n - c_w m_w \Delta \bar{T}_w}{m_n \Delta t} \quad (4-$$

a)

where $\Delta \bar{T}_n$ and $\Delta \bar{T}_w$ are the average temperature increases of GNPs dispersions and DI water at the same time interval, respectively. The time interval for SAR calculation is the same as that in the calculation of PTE. SAR (Fig. 7) decreases with the increase of the nanoparticle concentration, which is consistent with those from previous studies under non-focused solar radiation [34,35]. An impressive high value of 50 kW/g for gold nanoparticles with a

concentration of 1.02 ppm is achieved under 220 Suns solar radiation, which suggests that the absorbed solar energy by one gram of gold nanoparticles in only 3 seconds is more than the released thermal energy of 10 L hydrogen combustion under standard temperature and pressure conditions (i.e., $T=273\text{ K}$ and $P=1\text{ atm}$) [36].

3.4. Steam generation mechanisms

The experimental results clearly show that employing gold nanoparticles can significantly increase the absorption of solar energy, leading to more efficient steam generation. The experimental results are similar to those reported from the research group from Rice University [11,30]. However, there is no evidence to support the claim that steam production was caused by nanobubbles, i.e., bubbles were formed on top of heated nanoparticles. It should be noted that the solar intensity employed here was 220 Suns, as a few previous work [17,37–41] has suggested that nanobubbles were unlikely to be generated under relatively low heat fluxes. For example, both Kotaidis et al. [42] and Koblinski et al. [43] pointed out that a laser power density equivalent to more than 3×10^7 Suns was required to form nanobubbles. We explore possible steam generation mechanisms below.

3.4.1 Classical Nucleation and Heat Transfer Analysis

Bubble nucleation depends strongly on the morphology of the heated surface. Usually, surfaces have tiny pits and scratches can act as active nucleation sites, where embryonic bubbles can easily form. From the classical nucleation theory, the radius of the mouth of a cavity determines the superheat required for the vapor bubble to nucleate at that site [44] according to:

$$\Delta T = T_l - T_{\text{sat}} = \frac{T_{\text{sat}} v_{\text{fg}}}{h_{\text{fg}}} \left[\frac{2\sigma}{r_c} \right] \quad (5)$$

where $\Delta T = T_l - T_{\text{sat}}$ is the excess heating (superheating), v_{fg} , h_{fg} , σ are the specific volume difference between the vapor and liquid, latent heat of vaporization, and surface tension respectively at the saturation temperature T_{sat} , and r_c is the radius of a cavity mouth. It was found that the surface tension calculated by Young-Laplace equation ($\Delta p = \frac{2\sigma}{r}$, where Δp is the pressure difference across a spherical bubble and r is the radius of the bubble) is independent on the bubble size and agrees with the surface tension of a plane interface [45–47]. For a nanoparticle (i.e., $r = 10$ nm, as shown in Fig. 1) to act as an active nucleation site, 2400 °C superheat and a Laplace pressure difference of ~ 120 atm will be needed. Much higher superheat is needed if the bubble embryo is first formed on some defects on the nanoparticle surfaces. Clearly to initiate bubbles on top of nanoparticles, extremely high nanoparticle temperature is required according to the non-homogeneous nucleation theory.

As it is rather difficult to measure directly the nanoparticle surface temperature, a 3-D heat transfer model with isolated boundary conditions, was established and solved for a single gold nanoparticle immersed in water (see Supporting Information), corresponding to the experimental conditions (220 Suns, $I=220 \times 0.94 \text{ kW/m}^2 \approx 206 \text{ kW/m}^2$, $f_v = 12.75$ ppm, $D = 20$ nm). A global temperature rise (Fig. 8) within the fluid is observed and the temperature difference between the nanoparticle and surrounding water is rather small, i.e., at an order of 10^{-6} K. This can be explained by the classical heat transfer theory. The Fourier number, which is a dimensionless parameter that characterizes transient heat conduction, is very high (i.e., almost 10000 for the present work) at the nanoscale, which leads to a rapid establishment of a steady state temperature distribution around the nanoparticle only in a few seconds. At the macroscopic measurable timescale, the temperature difference between the nanoparticle and the surrounding fluid is negligible.

Clearly classical nucleation and heat transfer theory does not support the formation of nanobubbles on top of nanoparticles at $< 1 \text{ MW/m}^2$ that is typical for a Fresnel Lens, albeit it may be possible under high fluence lasers (i.e., $> 1000 \text{ MW/m}^2$) [13,14,16,23,24].

3.4.2 Non-uniform temperature distribution

Experimental results indicated that the heating up and vaporization processes were highly non-equilibrium with highly non-uniform temperature distribution for GNP dispersions. Considering limited thermocouple measurement positions in the experiment, potential maximum temperature difference within the fluids could be much larger than those measured in this work. It is possible that nucleate boiling may be initiated at some superheated regions, leading to rapid steam production. To reveal the transient steam generation mechanism, a 3-D mathematical model was proposed based on the radiative transfer equation and conductive heat transfer equation coupled with the phase change assumptions (detailed in Supporting Information). In the model, the absorption and scattering coefficients were calculated based on the Mie scattering theory [48] and the spectral intensity was described by the radiative transfer equation. A simplified 3-D transient conductive heat transfer equation with phase change and without consideration of the effects of gravity and two-phase flow, was used to obtain the temperature field within the fluid. The set of equations was numerically solved by COMSOL.

Corresponding to the experimental conditions, Fig. 9A shows an example of non-uniform temperature increases in 3 minutes for 1.02 ppm GNPs dispersion. Once the fluid is illuminated, its temperature increases immediately. The temperature of a small area near the top surface of the

tube reaches nearly 100 °C within 30 s, and a large temperature difference (i.e., 55 °C) can be observed during that period. The temperature of most fluid reaches higher than 90 °C after ~150 s, which is in good agreement with the experimental results shown in Fig. 3A. There is clearly a superheated region (i.e., temperature higher than 100 °C), which appears after 75 s and is represented as gray area in the figure. In this region, water could be possibly boiled or vaporized to steam, and a typical superheat of 5 °C was chosen in the mathematical model. In order to simplify the mathematical model, no fluid flow (due to buoyancy force and phase change) was considered. For bulk fluid boiling to occur (especially when the superheated region extends to the thermocouple wires), only a few degrees of superheat are needed, and the active nucleation sites could be from either the inner surface of the tube or the thermocouple wires, which is supported by our experimental observations. Clearly conventional bulk fluid boiling may occur within this superheated layer, leading to rapid steam production. For a high nanoparticle concentration (12.75 ppm, Fig. 9B), the illuminated area reaches the boiling point in only 9 seconds, which can lead to a nearly instant production of steam, albeit the bulk fluid still remains at the initial temperature. The simulation results support the experimental observations in Fig. 3C, where steam was generated (measured air temperature inside the tube began to increase) shortly after the GNP dispersion was illuminated under 220 Suns. The simulation results agree qualitatively with the experimental data. In addition to possible bulk boiling from the superheated region, strong vaporization at the fluid-air interface could also be responsible for some steam generation, especially before the boiling is initiated in the superheated region.

Both experimental and numerical results show that the mechanism responsible for solar steam generation of nanoparticle-based volumetric receivers is not due to the nanobubble formation, but because of extremely localized solar absorption in the focal area, where a superheated region

is easily formed and highly non-uniform temperature distribution exists within the fluid. With the increase of the volume concentration of GNP dispersions, more solar energy is localized at the top surface of the receiver, leading to stronger boiling and surface vaporization in the superheated region, although the bulk fluid is still in the subcooled state. However, such a subcooled state is not at the nanoscale, but at the bulk scale. Classical heat transfer theory is appropriate to explain the nanoparticle-based steam generation process. This supports the idea of employing nanoparticles to increase the efficiency of trapping solar energy. Clearly to produce steam more efficiently, future solar receiver design should focus more solar energy in the superheat region while minimizing the temperature rise of bulk fluid.

4. Conclusions

This work investigated the steam generation mechanism of gold nanoparticles-based solar volumetric receivers. Experiments were performed for GNP dispersions in cylindrical tubes under focused natural sunlight conditions, and 3-D numerical models were also established to simulate the temperature profile within the sample fluid and the heat transfer between a single particle and the surrounding fluid. It is found that steam generation of nanoparticle-based volumetric solar receivers is not due to the nanobubble formation on top of heated particles, but caused by a highly localized solar absorption in the focal area where intense boiling and vaporization occur, while considerable non-uniform temperature distribution within the fluid may exist in the heating-up stage. By increasing the volume concentration of GNP dispersions, more solar radiation energy is localized at the top surface of the receiver, leading to stronger boiling and surface vaporization in the superheated region, although the bulk fluid is still in the subcooled state. Under a solar concentration of 220 Suns, 12.75 ppm gold nanoparticles

dispersion can achieve a photothermal conversion efficiency up to 80.3%, and a specific absorption rate of ~ 50 kW/g at a concentration of 1.02 ppm can be reached. The work reveals that in the future solar receiver design, more solar energy should be focused and trapped in the superheated region while minimizing the temperature rise of the bulk fluid.

Author contributions

The manuscript was written through contributions of all authors. HJ performed experiments and simulation under instructions, GL and LB provided supervision for the work in Beihang University, LB and AZ provided useful discussions, and DW revealed steam generation mechanisms and provided overall quality control. All authors have given approval to the final version of the manuscript.

Acknowledgments

This work was supported by the EU Marie Curie Actions-International Incoming Fellowships (FP7-PEOPLE-2013-IIF-626576), and the author Haichuan Jin also acknowledges the financial support for his visiting study at the University of Leeds from the China Scholarship Council (CSC) under the Grant No.201506020031.

Appendix A. Supplementary materials

Supplementary data associated with this article can be found in the online version.

- I. Video showing bubble growth and boiling
- II. Uncertainty analysis for experimental results

III. Heat transfer model for nanoparticle immersed in water

IV. 3-D radiative heat transfer model

References

- [1] M.A. Shannon, P.W. Bohn, M. Elimelech, J.G. Georgiadis, B.J. Mariñas, A.M. Mayes, Science and technology for water purification in the coming decades., *Nature*. 452 (2008) 301–10. doi:10.1038/nature06599.
- [2] M. Elimelech, W.A. Phillip, The future of seawater desalination: energy, technology, and the environment., *Science*. 333 (2011) 712–7. doi:10.1126/science.1200488.
- [3] M.K. Gupta, S.C. Kaushik, Exergy analysis and investigation for various feed water heaters of direct steam generation solar–thermal power plant, *Renew. Energy*. 35 (2010) 1228–1235. doi:10.1016/j.renene.2009.09.007.
- [4] G.N. Tiwari, H.N. Singh, R. Tripathi, Present status of solar distillation, *Sol. Energy*. 75 (2003) 367–373.
- [5] S. Yu, Y. Zhang, H. Duan, Y. Liu, X. Quan, P. Tao, et al., The impact of surface chemistry on the performance of localized solar-driven evaporation system, *Sci. Rep.* 5 (2015) 13600. doi:10.1038/srep13600.
- [6] K. Bae, G. Kang, S.K. Cho, W. Park, K. Kim, W.J. Padilla, Flexible thin-film black gold membranes with ultrabroadband plasmonic nanofocusing for efficient solar vapour generation, *Nat. Commun.* 6 (2015) 10103. doi:10.1038/ncomms10103.
- [7] M.A. Shannon, Water desalination: Fresh for less., *Nat. Nanotechnol.* 5 (2010) 248–50. doi:10.1038/nnano.2010.71.

- [8] M. Elimelech, W.A. Phillip, The future of seawater desalination: energy, technology, and the environment., *Science*. 333 (2011) 712–7. doi:10.1126/science.1200488.
- [9] O.A. Yeshchenko, N. V. Kutsevol, A.P. Naumenko, Light-Induced Heating of Gold Nanoparticles in Colloidal Solution: Dependence on Detuning from Surface Plasmon Resonance, *Plasmonics*. 11 (2016) 345–350. doi:10.1007/s11468-015-0034-z.
- [10] T.K. Tullius, Y. Bayazitoglu, Temperature of a metallic nanoparticle embedded in a phase change media exposed to radiation, *Int. J. Heat Mass Transf.* 93 (2016) 980–990. doi:10.1016/j.ijheatmasstransfer.2015.10.038.
- [11] O. Neumann, A.S. Urban, J. Day, S. Lal, P. Nordlander, N.J. Halas, Solar vapor generation enabled by nanoparticles, *ACS Nano*. 7 (2013) 42–49. doi:10.1021/nn304948h.
- [12] J.M. McMahon, A.I. Henry, K.L. Wustholz, M.J. Natan, R.G. Freeman, R.P. Van Duyne, et al., Gold nanoparticle dimer plasmonics: Finite element method calculations of the electromagnetic enhancement to surface-enhanced raman spectroscopy, *Anal. Bioanal. Chem.* 394 (2009) 1819–1825. doi:10.1007/s00216-009-2738-4.
- [13] A.O. Govoroy, H.H. Richardson, Generating heat with metal nanoparticles, *Nano Today*. 2 (2007) 30–38. doi:10.1016/S1748-0132(07)70017-8.
- [14] E. Ye, K.Y. Win, H.R. Tan, M. Lin, C.P. Teng, A. Mlayah, et al., Plasmonic gold nanocrosses with multidirectional excitation and strong photothermal effect, *J. Am. Chem. Soc.* 133 (2011) 8506–8509. doi:10.1021/ja202832r.
- [15] V. Bianco, O. Manca, S. Nardini, K. Vafai, Heat transfer enhancement with nanofluids, CRC Press, Taylor and Francis Group, 2015.

- [16] E. Lukianova-Hleb, Y. Hu, L. Latterini, L. Tarpani, S. Lee, R.A. Drezek, et al., Plasmonic nanobubbles as transient vapor nanobubbles generated around plasmonic nanoparticles., *ACS Nano*. 4 (2010) 2109–23. doi:10.1021/nn1000222.
- [17] Z. Fang, Y.R. Zhen, O. Neumann, A. Polman, F.J. García De Abajo, P. Nordlander, et al., Evolution of light-induced vapor generation at a liquid-immersed metallic nanoparticle, *Nano Lett.* 13 (2013) 1736–1742. doi:10.1021/nl4003238.
- [18] H. Ghasemi, G. Ni, A.M. Marconnet, J. Loomis, S. Yerci, N. Miljkovic, et al., Solar steam generation by heat localization, *Nat. Commun.* 5 (2014) 1–7. doi:10.1038/ncomms5449.
- [19] X. Chen, A. Munjiza, K. Zhang, D. Wen, Molecular Dynamics Simulation of Heat Transfer from a Gold Nanoparticle to a Water Pool, *J. Phys. Chem. C*. 118 (2014) 1285–1293. doi:org/10.1021/jp410054j.
- [20] G. Baffou, R. Quidant, F.J. García De Abajo, Nanoscale control of optical heating in complex plasmonic systems, *ACS Nano*. 4 (2010) 709–716. doi:10.1021/nn901144d.
- [21] J.S. Donner, G. Baffou, D. McCloskey, R. Quidant, Plasmon-assisted optofluidics, *ACS Nano*. 5 (2011) 5457–5462. doi:10.1021/nn200590u.
- [22] G. Lajoinie, E. Gelderblom, C. Chlon, M.B. ouml Hmer, W. Steenbergen, N. de Jong, et al., Ultrafast vapourization dynamics of laser-activated polymeric microcapsules, *Nat. Commun.* 5 (2014) 1–8. doi:10.1038/ncomms4671.
- [23] H. Ma, P.M. Bendix, L.B. Oddershede, Large-scale orientation dependent heating from a single irradiated gold nanorod, *Nano Lett.* 12 (2012) 3954–3960. doi:10.1021/nl3010918.
- [24] G. Baffou, P. Bon, J. Savatier, J. Polleux, M. Zhu, M. Merlin, et al., Thermal imaging of

- nanostructures by quantitative optical phase analysis, *ACS Nano*. 6 (2012) 2452–2458.
doi:10.1021/nn2047586.
- [25] E.Y. Lukianova-Hleb, A.N. Volkov, D.O. Lapotko, Laser pulse duration is critical for the generation of plasmonic nanobubbles, *Langmuir*. 30 (2014) 7425–7434.
doi:10.1021/la5015362.
- [26] L. Hou, M. Yorulmaz, N.R. Verhart, M. Orrit, Explosive formation and dynamics of vapor nanobubbles around a continuously heated gold nanosphere, *New J. Phys.* 17 (2015) 13050. doi:10.1088/1367-2630/17/1/013050.
- [27] J. Vera, Y. Bayazitoglu, Temperature and heat flux dependence of thermal resistance of water/metal nanoparticle interfaces at sub-boiling temperatures, *Int. J. Heat Mass Transf.* 86 (2015) 433–442. doi:10.1016/j.ijheatmasstransfer.2015.02.033.
- [28] D. Wen, Intracellular hyperthermia: Nanobubbles and their biomedical applications., *Int. J. Hyperthermia*. 25 (2009) 533–41. doi:10.3109/02656730903061617.
- [29] G. Ni, N. Miljkovic, H. Ghasemi, X. Huang, S. V. Boriskina, C. Te Lin, et al., Volumetric solar heating of nanofluids for direct vapor generation, *Nano Energy*. 17 (2015) 290–301. doi:10.1016/j.nanoen.2015.08.021.
- [30] O. Neumann, C. Feronti, A.D. Neumann, A. Dong, K. Schell, B. Lu, et al., Compact solar autoclave based on steam generation using broadband light-harvesting nanoparticles., *Proc. Natl. Acad. Sci. U. S. A.* 110 (2013) 11677–81. doi:10.1073/pnas.1310131110.
- [31] H.-J. Chen, D. Wen, Ultrasonic-aided fabrication of gold nanofluids., *Nanoscale Res. Lett.* 6 (2011) 198. doi:10.1186/1556-276X-6-198.

- [32] C.-F.J. Kuo, C.-C. Huang, Y.-L. Kuo, Analysis of processing parameters in fabrication of Fresnel lens solar collector, *Energy Convers. Manag.* 57 (2012) 33–41. doi:10.1016/j.enconman.2011.12.003.
- [33] M. Mehrali, E. Sadeghinezhad, S. Latibari, S. Kazi, M. Mehrali, M.N.B.M. Zubir, et al., Investigation of thermal conductivity and rheological properties of nanofluids containing graphene nanoplatelets, *Nanoscale Res. Lett.* 9 (2014) 15. doi:10.1186/1556-276X-9-15.
- [34] E.P. Bandarra Filho, O.S.H. Mendoza, C.L.L. Beicker, A. Menezes, D. Wen, Experimental investigation of a silver nanoparticle-based direct absorption solar thermal system, *Energy Convers. Manag.* 84 (2014) 261–267. doi:10.1016/j.enconman.2014.04.009.
- [35] H. Zhang, H.J. Chen, X. Du, D. Wen, Photothermal conversion characteristics of gold nanoparticle dispersions, *Sol. Energy.* 100 (2014) 141–147. doi:10.1016/j.solener.2013.12.004.
- [36] P.J. Linstrom, W.G. Mallard, NIST Chemistry WebBook; NIST Standard Reference Database No. 69, Gaithersburg MD, 2001. <http://webbook.nist.gov/>.
- [37] M.T. Carlson, A.J. Green, H.H. Richardson, Superheating water by CW excitation of gold nanodots., *Nano Lett.* 12 (2012) 1534–7. doi:10.1021/nl2043503.
- [38] N.J. Hogan, A.S. Urban, C. Ayala-Orozco, A. Pimpinelli, P. Nordlander, N.J. Halas, Nanoparticles heat through light localization., *Nano Lett.* 14 (2014) 4640–5. doi:10.1021/nl5016975.
- [39] J. Lombard, T. Biben, S. Merabia, Kinetics of nanobubble generation around overheated

- nanoparticles., Phys. Rev. Lett. 112 (2014) 105701.
doi:10.1103/PhysRevLett.112.105701.
- [40] S. Baral, A.J. Green, M.Y. Livshits, A.O. Govorov, H.H. Richardson, Comparison of vapor formation of water at the solid/water interface to colloidal solutions using optically excited gold nanostructures., ACS Nano. 8 (2014) 1439–48. doi:10.1021/nn405267r.
- [41] G. Baffou, J. Polleux, H. Rigneault, S. Monneret, Super-Heating and Micro-Bubble Generation around Plasmonic Nanoparticles under cw Illumination, J. Phys. Chem. C. 118 (2014) 4890–4898. doi:10.1021/jp411519k.
- [42] V. Kotaidis, C. Dahmen, G. von Plessen, F. Springer, A. Plech, Excitation of nanoscale vapor bubbles at the surface of gold nanoparticles in water., J. Chem. Phys. 124 (2006) 184702. doi:10.1063/1.2187476.
- [43] P. Keblinski, D.G. Cahill, A. Bodapati, C.R. Sullivan, T.A. Taton, Limits of localized heating by electromagnetically excited nanoparticles, J. Appl. Phys. 100 (2006) 054305. doi:10.1063/1.2335783.
- [44] M. Massoud, Engineering thermofluids: Thermodynamics, fluid mechanics, and heat transfer, Eng. Thermofluids Thermodyn. Fluid Mech. Heat Transf. (2005) 1–1119. doi:10.1007/b138870.
- [45] M. Matsumoto, K. Tanaka, Nano bubble—Size dependence of surface tension and inside pressure, Fluid Dyn. Res. 40 (2008) 546–553. doi:10.1016/j.fluiddyn.2007.12.006.
- [46] M. Matsumoto, T. Yamamoto, Initial Stage of Nucleate Boiling at Atomic Scale, in: ASME/JSME 2011 8th Therm. Eng. Jt. Conf., ASME, 2011: pp. T30057–T30057–7.

doi:10.1115/AJTEC2011-44435.

- [47] M. Matsumoto, Surface Tension and Stability of a Nanobubble in Water: Molecular Simulation, *J. Fluid Sci. Technol.* 3 (2008) 922–929. doi:10.1299/jfst.3.922.
- [48] M.F. Modest, *Radiative Heat Transfer*, Academic Press, 2003.

Vitae



Haichuan Jin obtained his bachelor's degree in Aircraft Environment and Life Support Engineering of Beihang University, Beijing, P.R. China. He is currently a Ph.D. candidate in Human Machine and Environment Engineering of Beihang University. During his studies in 2016, he focuses on the photothermal conversion process of solar energy in nanofluid, and is as a visiting student in the University of Leeds.



Guiping Lin received his B.Sc. degree in the engineering thermophysics (1986) and PhD degree in the Human-Machine & Environmental Engineering (1993) from the Beihang University, China. He is a professor in the School of Aeronautic Science and Engineering, Beihang University. He was a visiting scholar in the University of Stuttgart, Germany in 1996-1997. His current research interests include aircraft environmental control, high heat flux heat transfer, advanced heat transfer devices such as heat pipe, loop heat pipe and cryogenic loop heat pipe.



Lizhan Bai received his BSc and PhD degree in the Human-Machine & Environmental Engineering from Beihang University, China in 2005 and 2012 respectively. He is an associate professor in the School of Aeronautic Science and Engineering, Beihang University. He was a visiting scholar in the Georgia Institute of Technology in 2010-2011, and is a research fellow in the University of Leeds in 2014-2016. His current research interests include spacecraft thermal control, high heat flux heat transfer, advanced heat transfer devices such as heat pipe, loop heat pipe and cryogenic loop heat pipe, nanofluid heat transfer and solar thermal energy harvesting.



Aimen Zeiny received the B.Sc. and M.Sc. degree in the Mechanical Engineering from the University of Babylon in 1998 and 2001 respectively. He is a senior lecturer in the Mechanical Engineering Department – University of Kufa and a member in the International Energy and Environment Foundation, Najaf, Iraq. He has been awarded a scholarship from the Iraqi Ministry of Higher Education and Scientific research to get the PhD at the University of Leeds. His main areas of research interest are

Energy and Pollution and his PhD research topic is using nanofluids in solar refrigeration systems.



Dongsheng Wen is a Chair Professor in the School of Chemical and Process Engineering at the University of Leeds. He received his DPhil from the University of Oxford, and is the Fellow of Royal Society of Chemistry (FRSC), Energy Institute (FEI), and Institute of Nanotechnology (FION), a Chartered Engineer (CEng) and a Chartered Scientist (CSci). His research covers a wide spectrum of nanotechnology and engineering science, centered on developing novel nanomaterials for efficient energy applications. He has published 140 papers in peer-reviewed journals, and is a recipient of European Research Council

Consolidate Grant.

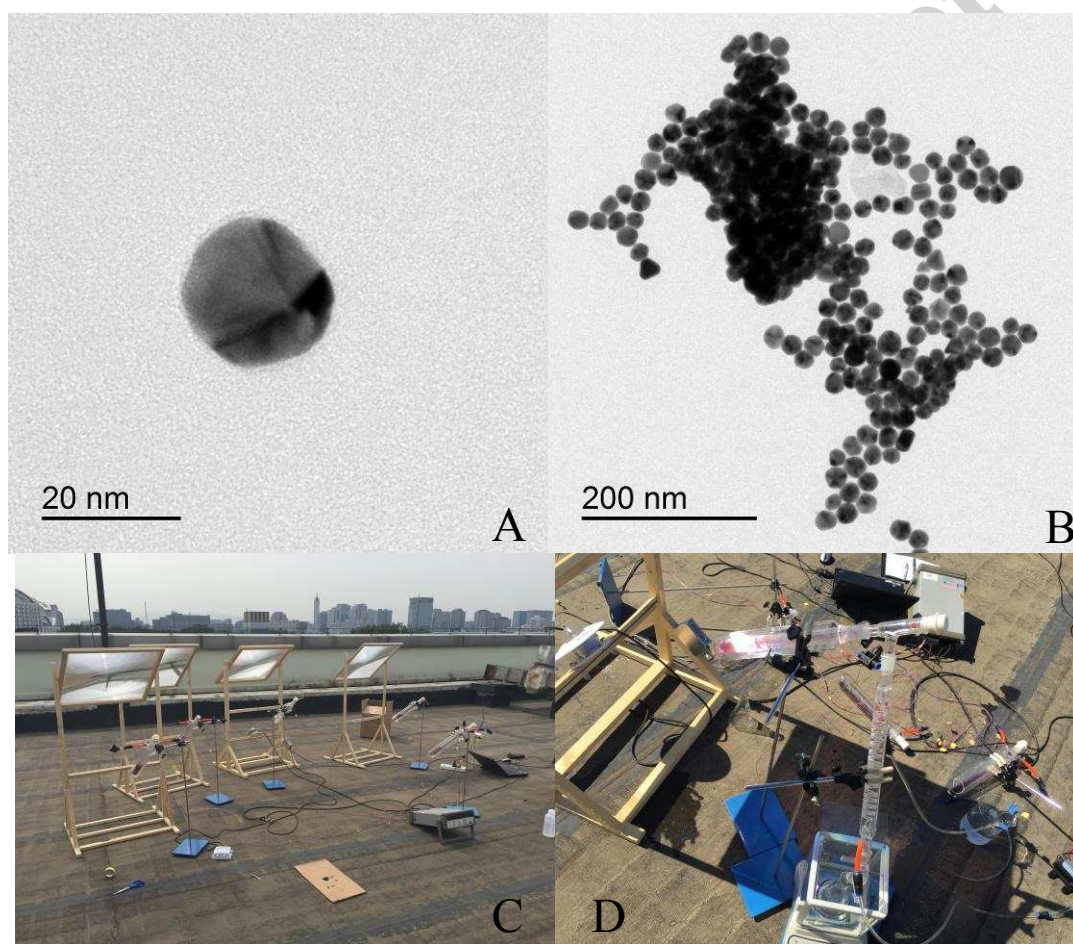


Fig. 1. (A) and (B) TEM images of gold nanoparticles; (C) Focused solar illumination experiment under natural sunlight conditions (located on the roof of Engineering Building in Beihang University in Beijing, $39^{\circ} 59' 5.49''$ North, $116^{\circ} 21' 18.70''$ East.), sun light is focused

220 times by a Fresnel Lens (400 mm × 400 mm) with a 620 mm focal distance; (D) Experimental setup for steam generation measurement.

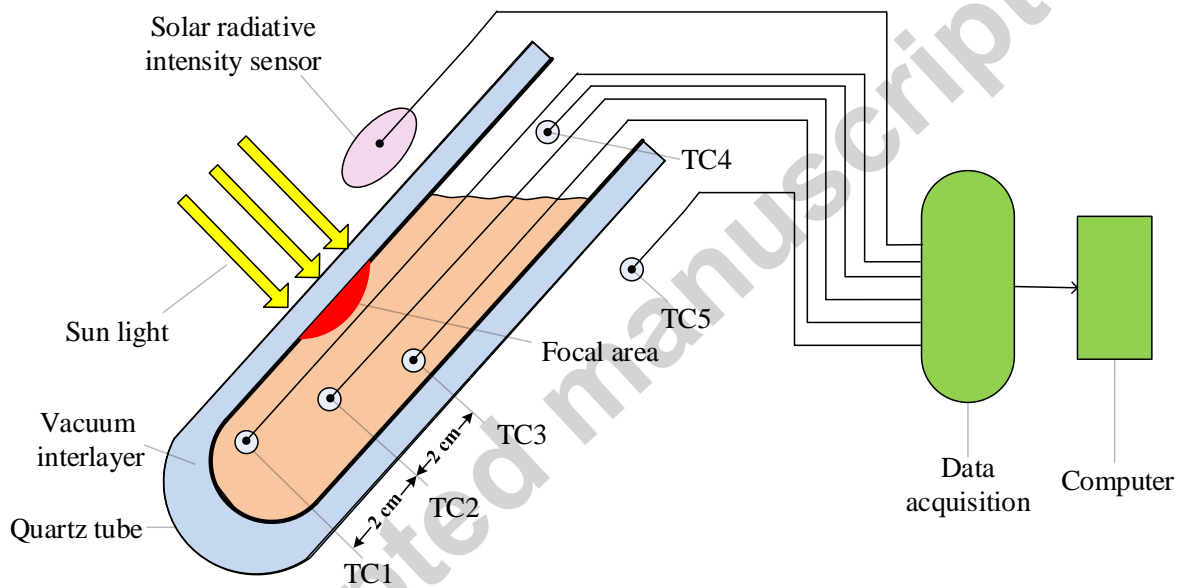


Fig. 2. A schematic view of the temperature measurement system. Three thermocouples were uniformly distributed along optical depth inside the nanofluids, respectively. Another two temperature sensors were placed inside and outside the tube to measure the evaporated steam and ambient temperature.

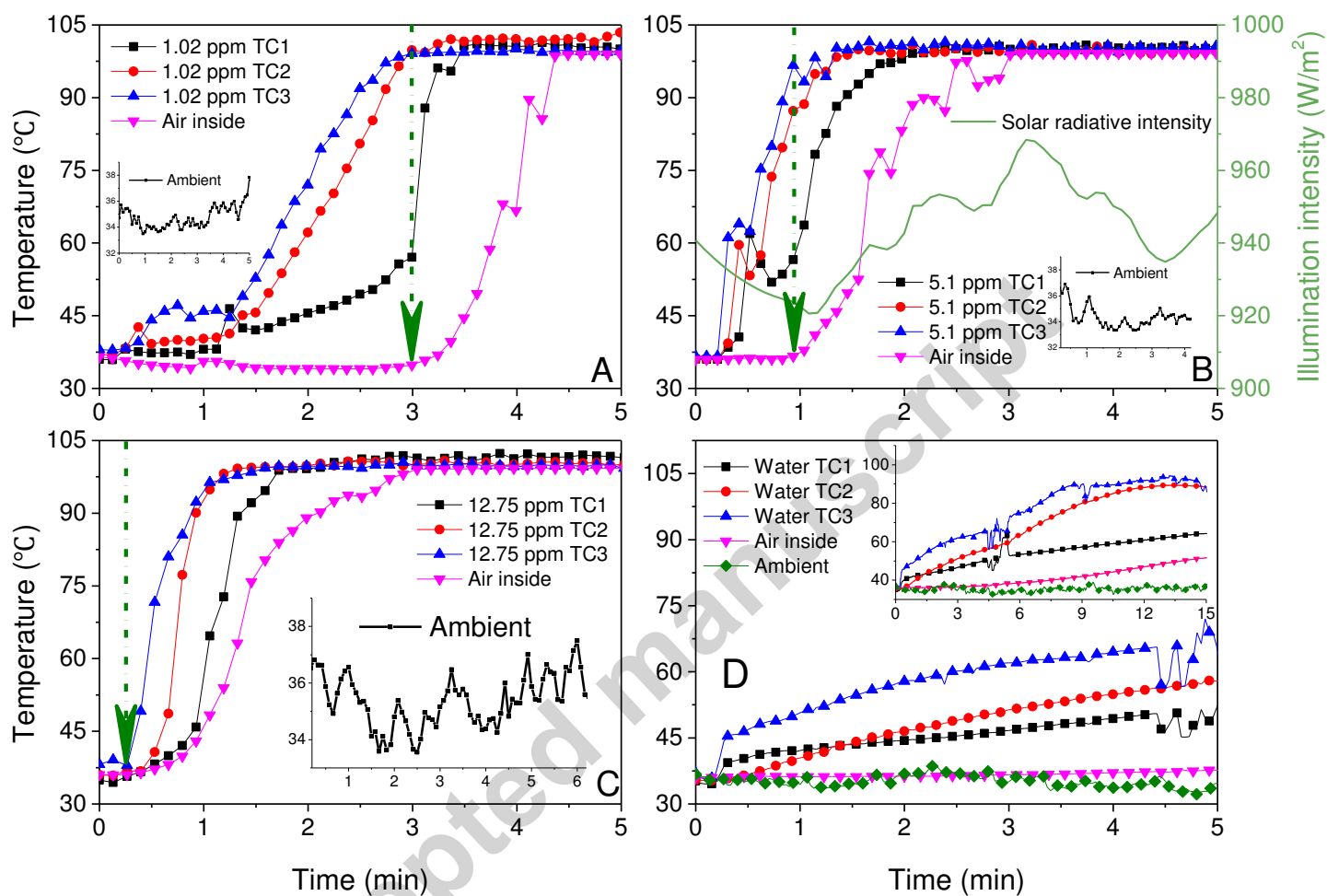


Fig. 3. Experimental results for GNPs dispersions with different volume concentrations and DI water. (A) 1.02 ppm; (B) 5.1 ppm; (C) 12.75 ppm; (D) DI water. Three thermocouples were employed to measure temperature of fluid inside the tube, another two measured the gas (or vapor) temperature inside the tube where the arrow shows the initial time of salient gas (or vapor) temperature increase, and the ambient temperature. Solar radiative intensity is also recorded as shown in (B).

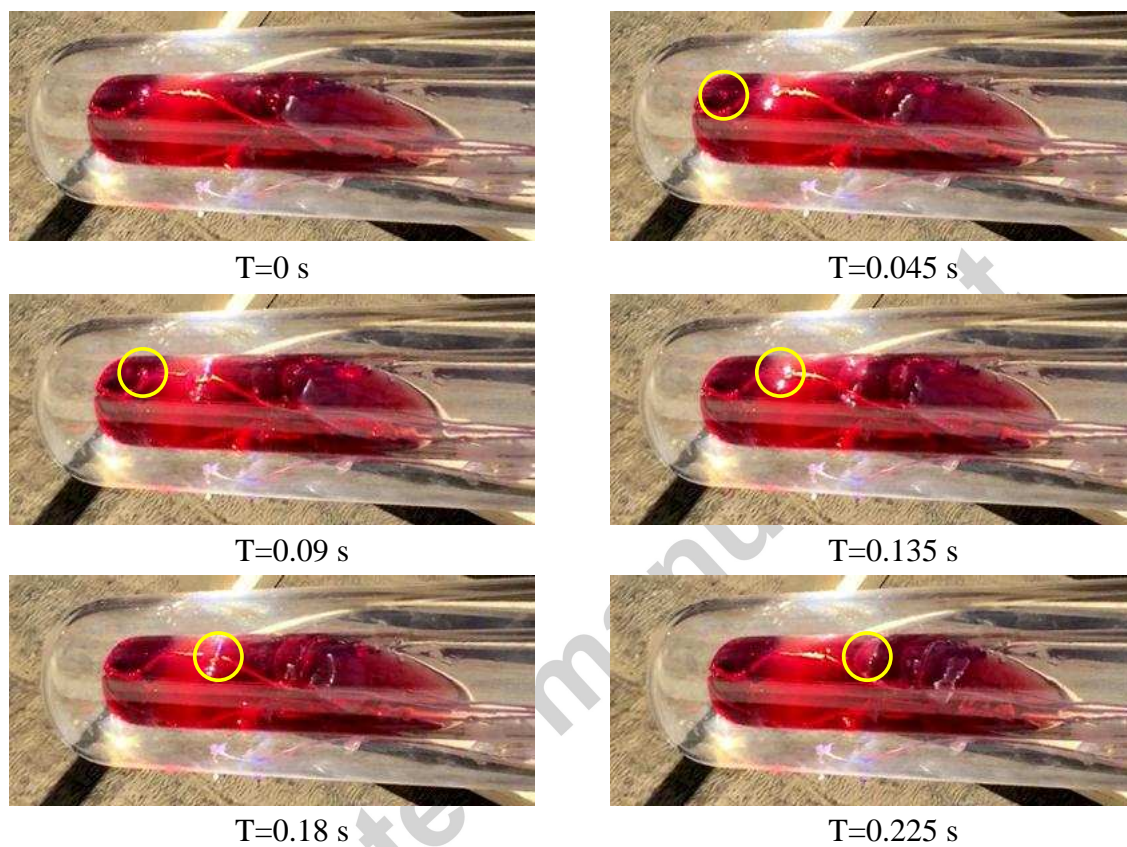


Fig. 4. Trace of one individual bubble in 0.225 s after 62 s solar illumination for 5.1 ppm gold nanofluid under 220 Suns, where each frame was taken every 0.045 s.

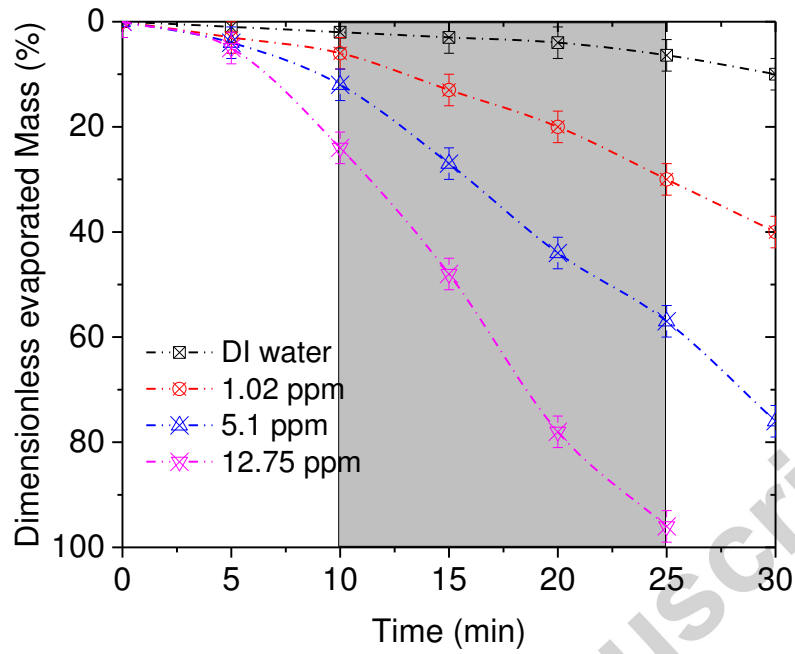


Fig. 5. Dimensionless mass change (the percentage mass loss) as a function of time for gold nanofluids and DI water illuminated by 220 Suns of radiation ($I=220 \times 0.94 \text{ kW/m}^2 \approx 206 \text{ kW/m}^2$); Stable mass change rate happens in gray zone.

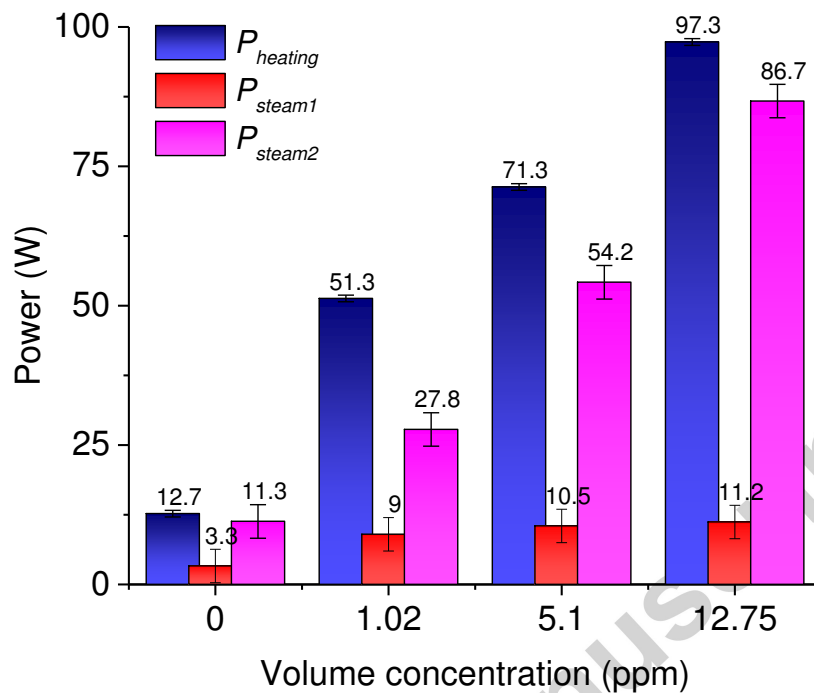


Fig. 6. Calculated power consumption for fluid heating (blue, $P_{heating1}$) determined by temperature rise and steam generation (red, P_{steam1}) through mass loss before bulk boiling, and power consumption for steam generation (pink, P_{steam2}) during the saturated boiling period.

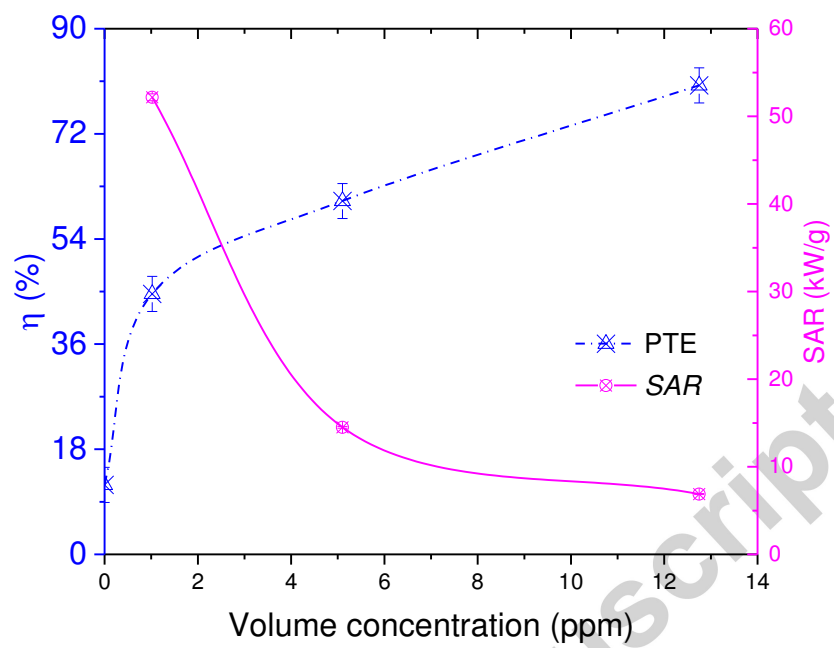


Fig. 7. Volume concentration dependence of photothermal conversion efficiency (η) and specific absorption rate (SAR) at the beginning of solar illumination.

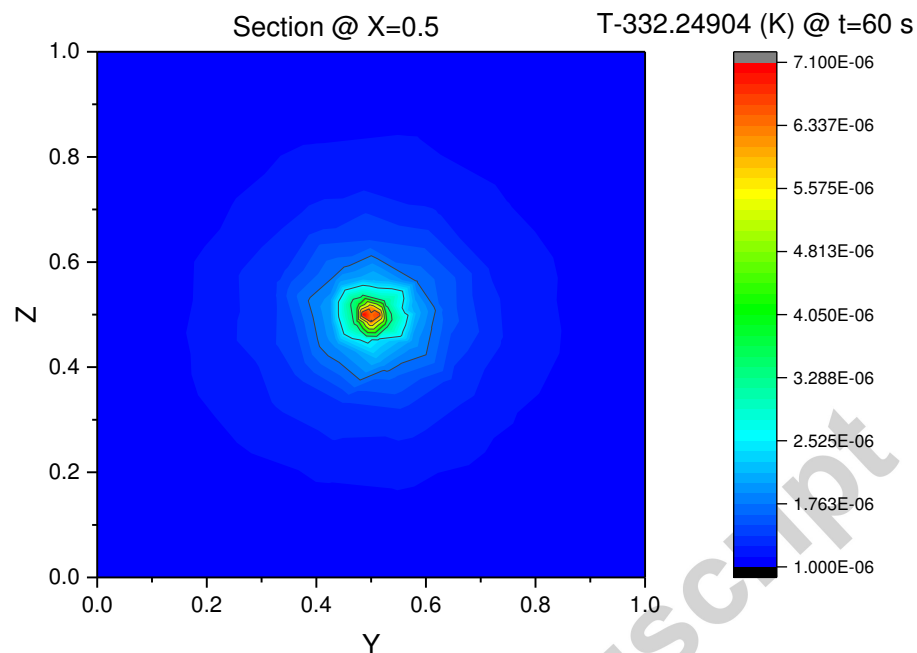


Fig. 8. Simulated temperature distribution between a single gold nanoparticle and surrounding water (in normalized distance) after 60 s illumination under 220 Suns for 12.75 ppm GNPs dispersion where label represents (T-332.24904) K.

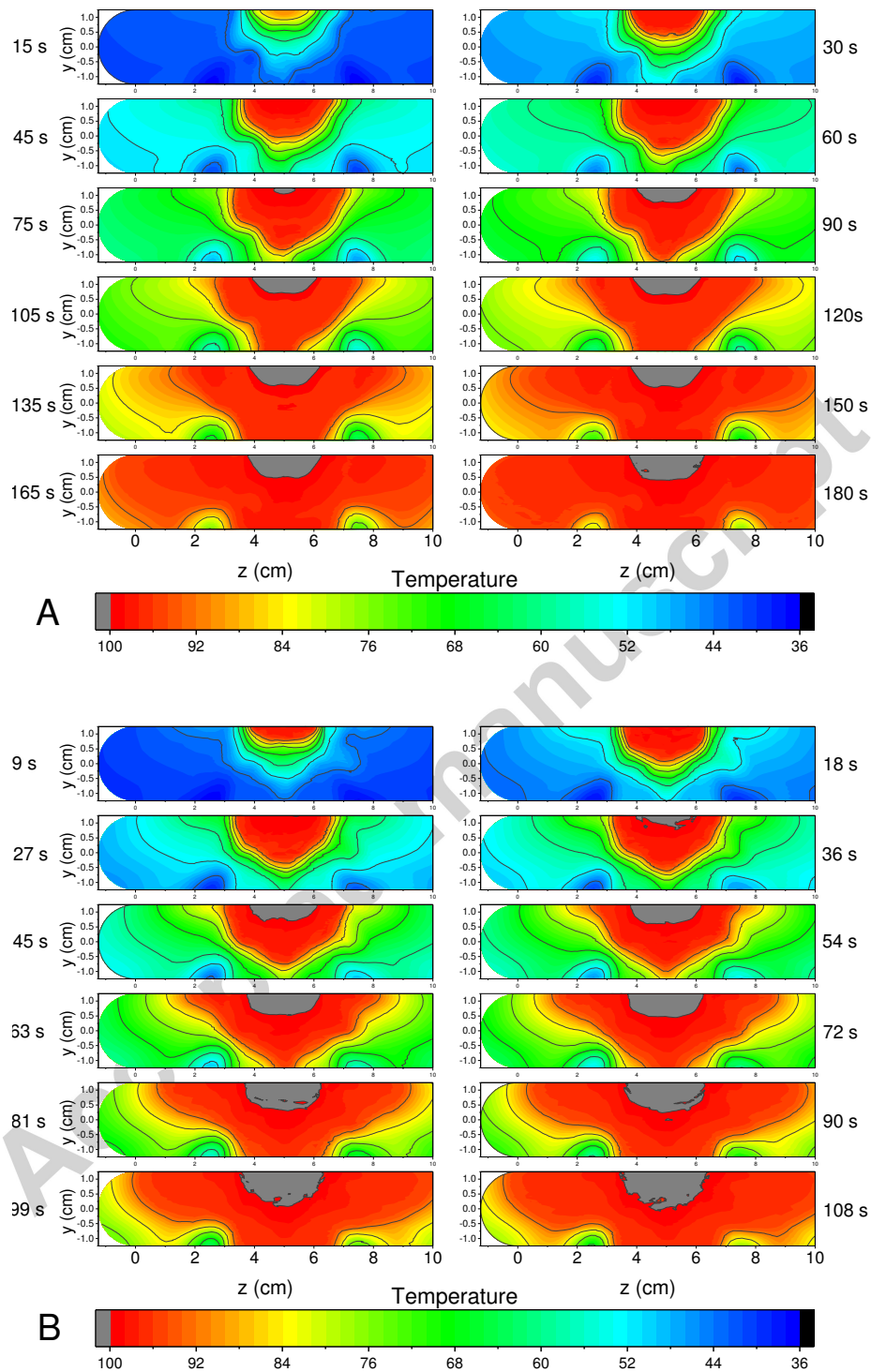


Fig. 9. Simulated temperature distribution evolutions with time for GNPs dispersions under 220 Suns illumination ($I=220 \times 0.94 \text{ kW/m}^2 \approx 206 \text{ kW/m}^2$) with different concentrations: (A) 1.02 ppm; (B) 12.75 ppm.

Table. 1 Sensible heating efficiency and steam generation efficiency in different periods

Samples	Before bulk boiling		Saturation boiling period	
	Sensible heating (3 thermocouples)	Sensible heating (only TC1)	Steam generation	Steam generation
DI water	9.4%	4.7%	2.5%	8.3%
1.02 ppm	37.9%	11.7%	6.7%	20.5%
5.1 ppm	52.7%	39.5%	7.8%	40.1%
12.75 ppm	71.9%	31.8%	8.3%	64.1%

Highlights

- Steam generation is due to boiling/vaporization in localized solar absorption area.
- Hypothesized nanobubble is unlikely to occur under normal solar concentrations.
- A photothermal efficiency of 80.3% was achieved for 12.75 ppm GNP dispersion
- A specific absorption rate of ~50 kW/g was achieved for 1.02 ppm GNP dispersion